Bioorganic Chemistry 96 (2020) 103637

Contents lists available at ScienceDirect

Bioorganic Chemistry

journal homepage: www.elsevier.com/locate/bioorg

Protostane-type triterpenoids as natural soluble epoxide hydrolase inhibitors: Inhibition potentials and molecular dynamics

Cheng-Peng Sun[a,*,1], Juan Zhang[a,b,1], Wen-Yu Zhao[a,1], Jing Yi[a], Jian-Kun Yan[d], Ya-Li Wang[c], Christophe Morisseau[e], Zhong-Bo Liu[c,*], Bruce D. Hammock[e,*], Xiao-Chi Ma[a]

[a] College of Pharmacy, College (Institute) of Integrative Medicine, The National & Local Joint Engineering Research Center for Drug Development of Neurodegenerative Disease, Dalian Medical University, Dalian, China
[b] School of Life Science, Liaoning Provincial Key Laboratory of Biotechnology and Drug Discovery, Liaoning Normal University, Dalian, China
[c] School of Pharmacy, Shenyang Pharmaceutical University, Shenyang, China
[d] Analysis Center of College of Science & Technology, Hebei Agricultural University, Cangzhou, Hebei, China
[e] Department of Entomology and Nematology, UC Davis Comprehensive Cancer Center, University of California, Davis, CA, USA

ARTICLE INFO

Keywords:
Soluble epoxide hydrolase
Protostane-type triterpenoids
Inhibition kinetics
Molecular dynamics stimulation

ABSTRACT

The inhibition of soluble epoxide hydrolase (sEH) is a promising therapeutic approach to treat inflammation and other disorders. In our present investigation on searching for sEH inhibitors from traditional Chinese medicines, we found that *Alisma orientale* displayed inhibition of sEH. We constructed a small library of protostane-type triterpenoids (**1**–**25**) isolated from *A. orientale*, and screened their inhibitory activities. Alismanin B (**1**), 11-deoxy-25-anhydro alisol E (**4**), 11-deoxy alisol B (**5**), and 25-*O*-ethyl alisol A (**15**) displayed concentration-dependently inhibitory activities against sEH with IC_{50} values from 3.40 ± 0.57 μM to 9.57 ± 0.88 μM. 11-Deoxy-25-anhydro alisol E (**4**) and 11-deoxy alisol B (**5**) were defined as mixed-type competitive inhibitors with Ki values of 12.6 and 3.48 μM, respectively, based on the result of inhibition kinetics. The potential interaction mechanism of 11-deoxy alisol B (**5**) with sEH was analyzed by molecular docking and molecular dynamics, revealing that amino acid residues Trp336 and Tyr466 were vital for its inhibitory activity.

1. Introduction

Soluble epoxide hydrolase (sEH, E.C. 3.3.2.10) is a bifunctional enzyme of the *α/β* hydrolase family. It possesses a *C*-terminal hydrolase activity and an *N*-terminal phosphatase activity [1,2]. The *C*-terminal epoxide hydrolase can hydrolyze a variety of epoxides [3–5], whereas the *N*-terminal lipid phosphatase acts on 12-phosphonooxy-octadec-9*Z*-enoic acid, *erythro*-9,10-phosphonooxy-hydroxy-octadecanoic acid, *threo*-9,10-phosphonooxy-hydroxy-octadecanoic acid, and 12-phosphonooxy-octadec-9*E*-enoic acid [3–5]. The *C*-terminal function of sEH has received the most attention since it can hydrolyze epoxides of arachidonic acid (AA) epoxy eicosatrienoic acids (EETs) via opening of the epoxide into a vicinal diol termed dihydroxy eicosatrienoic acids (DHETs) [6,7]. The inhibition of sEH is a method of elevating the concentration of EETs, EETs and other epoxy fatty acids (EpFA) have many effects including glycogen synthase kinase-3 beta (GSK3*β*) and nuclear factor kappa B (NF-*κ*B) inhibition. Inhibition of sEH exerts anti-inflammatory effects in Parkinson's disease and cardiovascular diseases [6,8–14]. Therefore, sEH is considered as a promising therapeutic approach for resolution of inflammation [15–17].

Recently, a collection of sEH inhibitors with varied skeleton, including ureas, amides, triterpenoids, and flavones, have come to light [18–23], which stimulated medicinal and natural product chemists to develop and discover more efficacious sEH inhibitors with excellent specificity and high safety profile [24–26]. To date, the most powerful of sEH inhibitors are ureas, such as *N*-[1-(1-oxopropyl)-4-piperidinyl]-*N*'-[4-(trifluoromethoxy)phenyl]urea (TPPU) and 12-[[(tricyclo [3.3.1.13,7]dec-1-ylamino)carbonyl]amino]-dodecanoic acid (AUDA), that can competitively bind to the epoxide binding in the catalytic site – Asp335, Tyr466, and Tyr383 [27–31]. Traditional Chinese medicines

* Corresponding authors.
E-mail addresses: suncp146@163.com (C.-P. Sun), 546265581@qq.com (Z.-B. Liu), bdhammock@ucdavis.edu (B.D. Hammock).
[1] These authors contributed equally to this work.

https://doi.org/10.1016/j.bioorg.2020.103637
Received 28 October 2019; Received in revised form 13 January 2020; Accepted 28 January 2020
Available online 29 January 2020

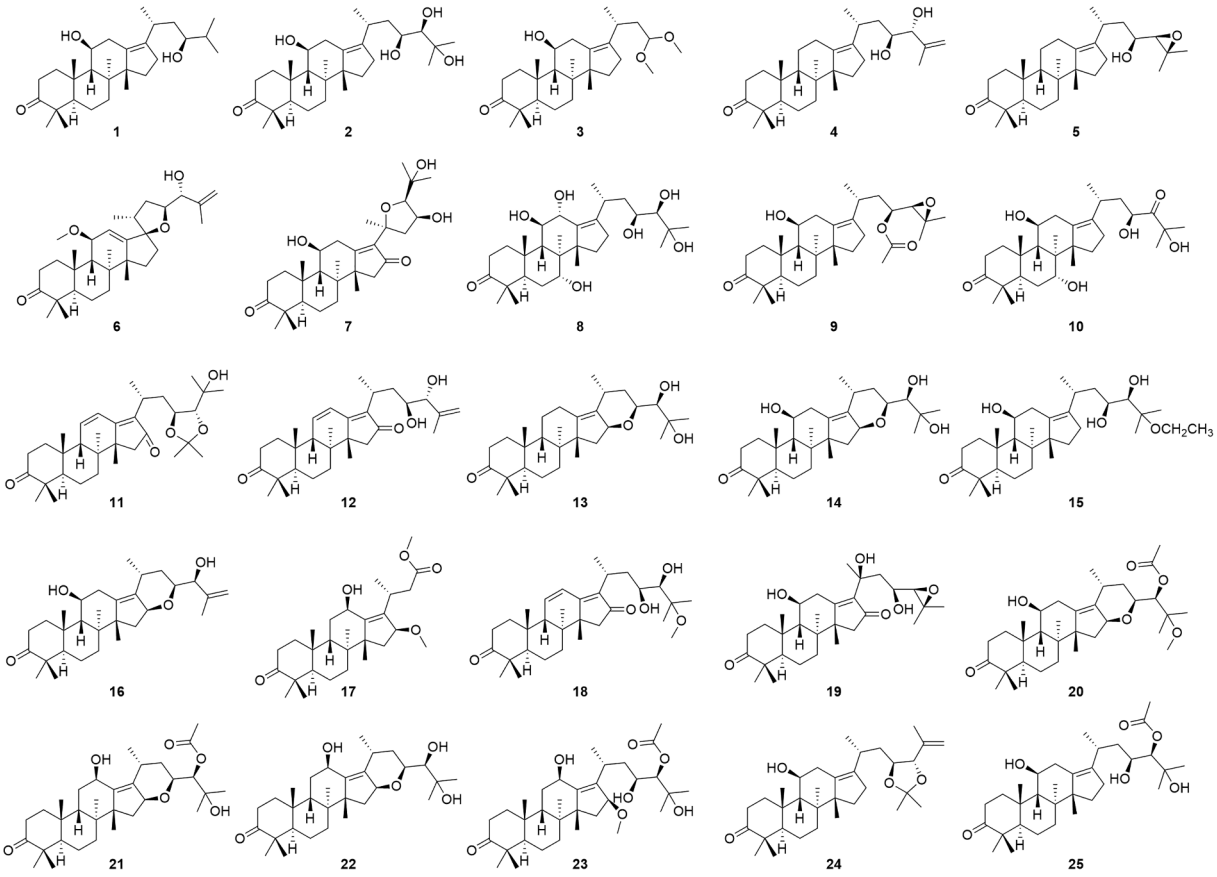

Fig. 1. The structures of twenty-five protostane-type triterpenoids.

are the important natural resources for medicine [32–35], which provides possibility of searching for the new generation of sEH inhibitors. This also raises the possibility of finding valuable natural supplements, meanwhile, *Alisma orientale* displayed the potential of inhibition on sEH, therefore, we collected twenty-five protostane-type triterpenoids (**1–25**, Fig. 1) from *A. orientale* and screened their inhibitory activities. 11-Deoxy alisol B (**5**) showed potent inhibitory activity against sEH, which stimulated us to further investigate its inhibition behavior and mechanism of action by molecular docking and molecular dynamics.

2. Results and discussion

2.1. sEH inhibitory effects

The mammalian microsomal has been well studied in xenobiotic metabolism. The sEH can degrade some xenobiotics or foreign compounds but it is best known for degrading biologically active, 1,2-disubstituted epoxides of fatty acids [19,23,28]. Some of potential sEH inhibitors have been isolated from traditional Chinese medicines or synthesized by chemists [15,19–23], including capsaicin, dihydrocapsaicin, piperlonguminine, dihydropiperlonguminine, futoamide, and urea analogues, stimulating us to screen the sEH inhibitors from natural products. We screened the inhibitory activities of twenty-five protostane-type triterpenoids (**1–25**) against sEH based on the method of sEH-mediated fluorogenic substrate PHOME hydrolysis [16,23]. As shown in the heatmap Fig. 2A and Table 1, compounds **1**, **3–6**, and **15** possessed potential inhibition on sEH activity (> 70%) at 50 μM, especially compound **5** (> 95%). Compounds **11**, **13**, **16**, **18**, **19**, **24**, and **25** could inhibit more than 50% sEH activity at the final concentration of 50 μM. In order to quantify the inhibitory potentials of triterpenoids on sEH, the relationship between inhibitor concentrations and inhibitory potential were plotted. Compounds **1**, **4**, **5**, and **15** could dose-dependently inhibit sEH activity, and their IC_{50} values were 7.15 ± 0.59, 5.94 ± 0.54, 3.40 ± 0.57, and 9.57 ± 0.88 μM, respectively (Fig. 2), whereas compounds **3**, **6**, **11**, **13**, **16**, **18**, **19**, **24**, and **25** displayed moderate inhibitory effects with IC_{50} values ranging from 14.3 ± 1.1 μM to 36.3 ± 4.0 μM.

The structures of triterpenoids **1–25** and IC_{50} values were used to analyze their structure-activity relationships. Comparison of IC_{50} values of compounds **2** with **15** and **12** with **18** revealed that the alkylation of C-25 hydroxy group was in favor of inhibitory activity. The IC_{50} value of compound **14** was more than 50 μM, whereas compound **13** displayed significant inhibitory activity with an IC_{50} value of 22.1 μM, which indicated that the C-11 hydroxy substitution negatively affected its inhibitory activity. An analogous case was also observed for compounds **5**, **9**, and **19**, compound **5** showed significant inhibitory activity (IC_{50} = 3.40 μM), whereas compounds **9** and **19** did not displayed significantly inhibitory activities. The dehydration of OH-25 in compound **14** led to the produce of compound **16**, and the latter displayed more inhibitory activity than the former, revealing that the $\Delta^{25(26)}$ olefinic bond was essential to inhibitory activity. The similar result was also observed for compounds **2** (IC_{50} > 50 μM) and **4** (IC_{50} = 5.94 μM). Compared with inhibitory efficiency of compounds **2** with **8** and compounds **13** with **22** suggested that the hydrolyzation of

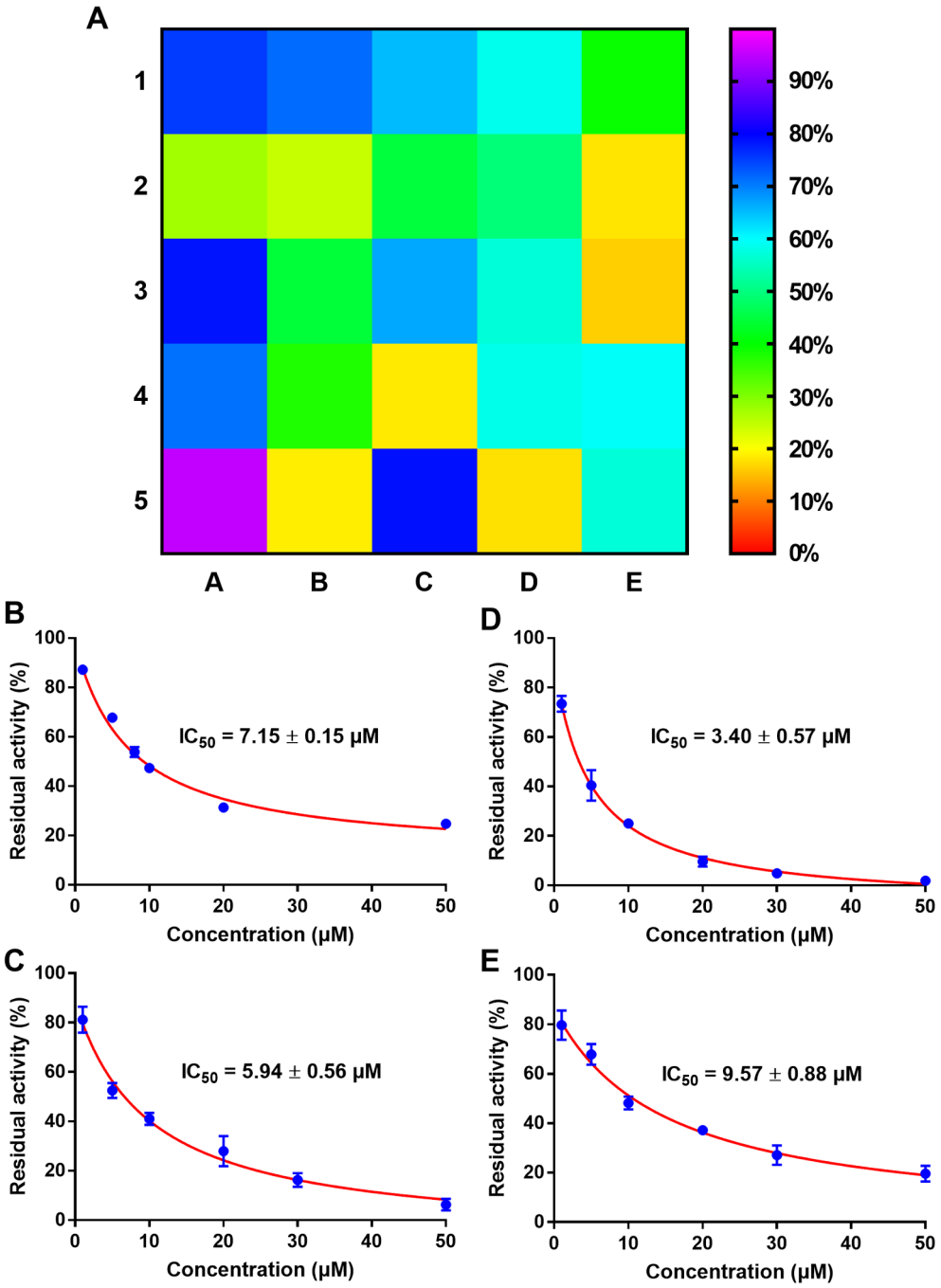

Fig. 2. (A) Compounds **1–25** (A1-A5, **1–5**; B1-B5, **6–10**; C1-C5, **11–15**; D1-D5, **16–20**; E1-E5, **21–25**) displayed inhibitory activities against sEH at 50 μM; (B-E) Compounds **1**, **4**, **5**, and **15** dose-dependently inhibited sEH activities *in vitro*.

C-7 and C-12 went against inhibitory activity. Additionally, the $\Delta^{25(26)}$ olefinic bond and 16-oxo group operated to the disadvantage of inhibitory activity via an analysis of inhibitory activities of compounds **4** and **12**.

2.2. Inhibition mechanism of compounds 4 and 5

The potent inhibitory activity of compounds **4** and **5** stimulated us to study their inhibition behaviors. Inhibition kinetics on compounds **4** and **5** were performed to assign the inhibition type which was competitive, mixed competitive, noncompetitive, or uncompetitive type on the basis of Michealis-Menten and Lineweaver-Burk plots (Fig. 3). Lineweaver-Burk plots clearly demonstrated that compounds **4** and **5** functioned as mixed-type competitive inhibitors against sEH in Fig. 3C and D showing that a series of lines were intersected at the second quadrant, and the inhibition constants (Ki) were defined as 12.6 and

Table 1
Inhibitory activities of compounds **1**–**25** against sEH.

Compounds	Inhibition of compounds against sEH	
	50 μM (%)	IC_{50} (μM)
1	75.31 ± 2.42	7.15 ± 1.09
2	27.33 ± 2.81	> 50
3	78.54 ± 1.86	14.8 ± 1.1
4	71.21 ± 1.56	5.94 ± 0.54
5	95.23 ± 1.24	3.40 ± 0.57
6	71.6 ± 2.12	14.6 ± 1.1
7	24.45 ± 1.03	> 50
8	44.42 ± 1.43	> 50
9	37.63 ± 0.86	> 50
10	18.64 ± 0.45	> 50
11	65.62 ± 1.65	36.3 ± 4.0
12	44.97 ± 0.95	> 50
13	66.84 ± 2.09	22.1 ± 1.4
14	18.30 ± 0.35	> 50
15	78.66 ± 2.19	9.57 ± 0.88
16	58.56 ± 1.31	21.2 ± 0.5
17	49.44 ± 1.15	> 50
18	56.93 ± 1.26	31.5 ± 1.4
19	58.34 ± 1.31	22.2 ± 1.0
20	17.63 ± 0.56	> 50
21	39.33 ± 0.92	> 50
22	17.96 ± 0.69	> 50
23	16.27 ± 0.72	> 50
24	59.45 ± 1.53	14.6 ± 1.6
25	56.98 ± 1.86	21.4 ± 1.7
TPPU[a]	–[b]	53 nM

[a] Positive control.
[b] No tested.

3.48 μM (Fig. 3E and F and Table 2), respectively.

2.3. Interaction analysis

The binding sites of compounds **4** and **5** with sEH were predicted by molecular docking on the basis of their inhibition kinetic results. Compounds **4** and **5** could bond to the catalytic cavity of sEH, and their lowest binding energies were −36.45 and −40.52 kcal/mol (Fig. 4 and Table 3), respectively. Compound **4** interacted with amino acid residues Asp335, Tyr383, and Tyr466 with the distances of 2.80, 2.59, and 2.68 Å through three hydrogen bonds, respectively. Compound **5** possessed two hydrogen bonds between the hydroxy group at C-23 and amino acid residues Trp336 and Tyr466 at the distances of 3.01 and 2.95 Å, respectively. Furthermore, compounds **4** and **5** also had hydrophobic interactions with other surrounding amino acid residues (Asp335, Met339, Thr343, Thr360, Ile363, Ala365, Pro371, Ile375, Phe381, Thr383, Gln384, Met469, Trp473, Val498, Leu499, and His524) of the catalytic pocket [21,23,26,27]. According to the above-mentioned results, the hydroxy group of C-23 and amino acid residue Tyr466 were critical for inhibitory activities of protostane-type triterpenoids against sEH.

2.4. Molecular dynamics

Because compound **5** showed potent inhibitory activity against sEH with Ki value of 3.48 μM and interacted with key amino acid residue Trp366 and Tyr466, therefore, we used Gromacs to investigate the molecular dynamics (MD) of compound **5** with sEH. The potential energy of the complex of sEH with compound **5** was held at about -2.16×10^6 kJ/mol during the simulation (Fig. 5). RMSD, a parameter to access the stability of the protein-ligand system [19,20,22], was also calculated, and the backbone RMSD of compound **5** was represented at a distance of about 3.5 Å during 10 ns of MD simulation (Fig. 5). RMSF of residues was acquired to figure out regions exhibiting higher flexibility with a distance of approximately 2.0 Å in MD simulation of compound **5** (Fig. 5). The number of hydrogen bonds and their distances throughout the MD simulation trajectory were determined using the gmx hbond and gmx distance tools in Gromacs. As shown in Fig. 5, compound **5** interacted with sEH via 1–3 hydrogen bonds during 10 ns of MD stimulation. The docking result indicated that amino acid residues Trp336 and Tyr466 could form hydrogen bonds with compound **5**, therefore, we analyzed the level of the interactions of compound **5** with the above-mentioned residues. In MD simulation of compound **5**, amino acid residue Trp336 was held at a distance of about 3.0 Å with the C-23 hydroxy group, amino acid residue Tyr466 was held at a distance of about 3.25 Å with the C-23 hydroxy group, which suggested that amino acid residues Trp336 and Tyr466 were vital for the inhibition of compound **5** against sEH. The above-mentioned result further supported the molecular docking result of compound **5**. This finding revealed that compound **5** could be regarded as a potential sEH inhibitor.

3. Conclusions

In summary, we screened the inhibitory potentials of twenty-five protostane-type triterpenoids against sEH, and compounds **1**, **4**, **5**, and **15** showed inhibition on sEH activity with IC_{50} values from 3.40 ± 0.57 μM to 9.57 ± 0.88 μM. Compounds **4** and **5** were assigned as mixed-type competitive inhibitors with Ki values of 12.6 and 3.48 μM, respectively. Molecular docking and molecular dynamics were used to analyze the potential interaction mechanism of compound **5** with sEH, suggesting that amino acid residues Trp336 and Tyr466 were vital for the inhibitory activity of compound **5**.

4. Material and methods

4.1. General experimental procedures

sEH protein was provided by the laboratory of Bruce D. Hammock in Department of Entomology and Nematology, UC Davis Comprehensive Cancer Center, University of California. Alismanin B (**1**), alisol A (**2**), alismanin D (**3**), 11-deoxy-25-anhydro alisol E (**4**), 11-deoxy alisol B (**5**), alismanin F (**6**), alismanol O (**7**), 7*α*,12*α*-dihydroxy-alisol A (**8**), alisol B 23-acetate (**9**), 7*α*-hydroxy-24-oxo alisol A (**10**), 16-oxo-11-anhydro alisol A 23,24-acetonide (**11**), alismanol B (**12**), 11-deoxy alisol F (**13**), alisol F (**14**), 25-*O*-ethyl alisol A (**15**), 25-anhydro alisol F (**16**), alismanin E (**17**), 25-ethoxy-16-oxo-11-anhydro alisol A (**18**), 20-hydroxy alisol C (**19**), 25-methoxy alisol F 23-acetate (**20**), 11-deoxy-12*β*-hydroxy alisol F 24-acetate (**21**), 11-deoxy-12*β*-hydroxy alisol F (**22**), 1-deoxy-12*β*-hydroxy-16*β*-methoxy alisol A 24-acetate (**23**), alisol G (23, 24)-diol acetonide (**24**), and alisol A 24-acetate (**25**) were isolated from *A. orientale* by the authors [35], their structures were identified by NMR and MS spectra, and their purities were more than 98% analyzed by HPLC.

4.2. sEH inhibitory activity

The inhibitory activities of compounds **1**–**25** against sEH were screened according to sEH-meditated probe substrate PHOME (Cayman Chemical, Ann Arbor, MI) hydrolysis [16,18]. Compounds **1**–**25** were

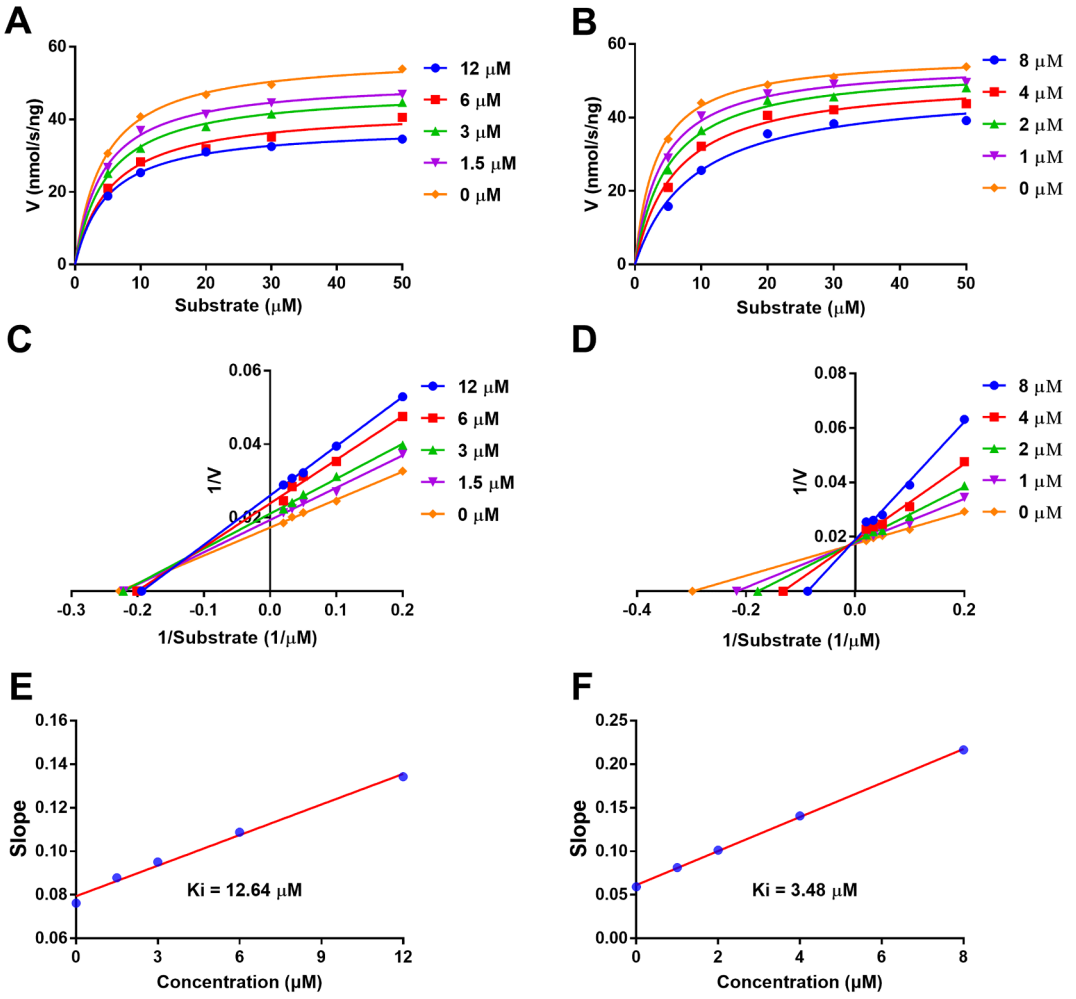

Fig. 3. (A-B) Michealis-Menten plots of compounds **4** and **5** against sEH. (C-D) Lineweaver-Burk plots of compounds **4** and **5** against sEH. (E-F) Slope plots of compounds **4** and **5** against sEH.

Table 2
Kinetic parameters of compounds **4** and **5** against sEH.

Compounds	Inhibition type	Ki (μM)	Goodness of fit (r)
4	mixed-type	12.6	0.9988
5	mixed-type	3.48	0.9974

added into the standard incubation system (200 μL), including sEH (0.1 ng/mL), BisTris-HCl buffer (pH 7.4, 25 mM), and probe PHOME (10 μM). The reaction was performed for 20 min at 37 °C, then the fluorescence signal at 465 nm was recorded. TPPU (Cayman Chemical, Ann Arbor, MI) was used as a positive control [23].

4.3. Inhibitory kinetic analysis

The inhibition kinetics of compounds **4** and **5** were performed by using Michealis-Menten analyses [23]. Their inhibition types (competitive inhibition, noncompetitive inhibition, uncompetitive inhibition, or mixed-type inhibition) were identified according to Lineweaver-Burk plots, and their inhibition constants (Ki) were calculated by slope plots and four inhibition kinetics models [Eq. (1): Competitive inhibition; Eq. (2): Noncompetitive inhibition; Eq. (3): Uncompetitive inhibition; Eq. (4): Mixed-type inhibition].

$$v = \frac{\text{Vmax}}{1 + \frac{\text{Km}}{[S]}(1 + \frac{[I]}{\text{Ki}})} \quad (1)$$

$$v = \frac{\text{Vmax}}{(1 + \frac{\text{Km}}{[S]})(1 + \frac{[I]}{\text{Ki}})} \quad (2)$$

$$v = \frac{\text{Vmax}}{1 + \frac{\text{Km}}{[S]} + \frac{[I]}{\text{Ki}})} \quad (3)$$

$$v = \frac{\text{Vmax}}{\frac{\text{Km}}{[S]}\left(1 + \frac{[I]}{\text{Ki}}\right) + 1 + \frac{[I]}{\text{Ki}}} \quad (4)$$

V, reaction rate; Vmax, maximum rate; Km, Michaelis constant, Ki, inhibition constant; S, the concentrations of substrate; I, the concentrations of inhibitor.

4.4. Molecular docking

The interactions of compounds **4** and **5** with sEH (PDB ID: 4OCZ)

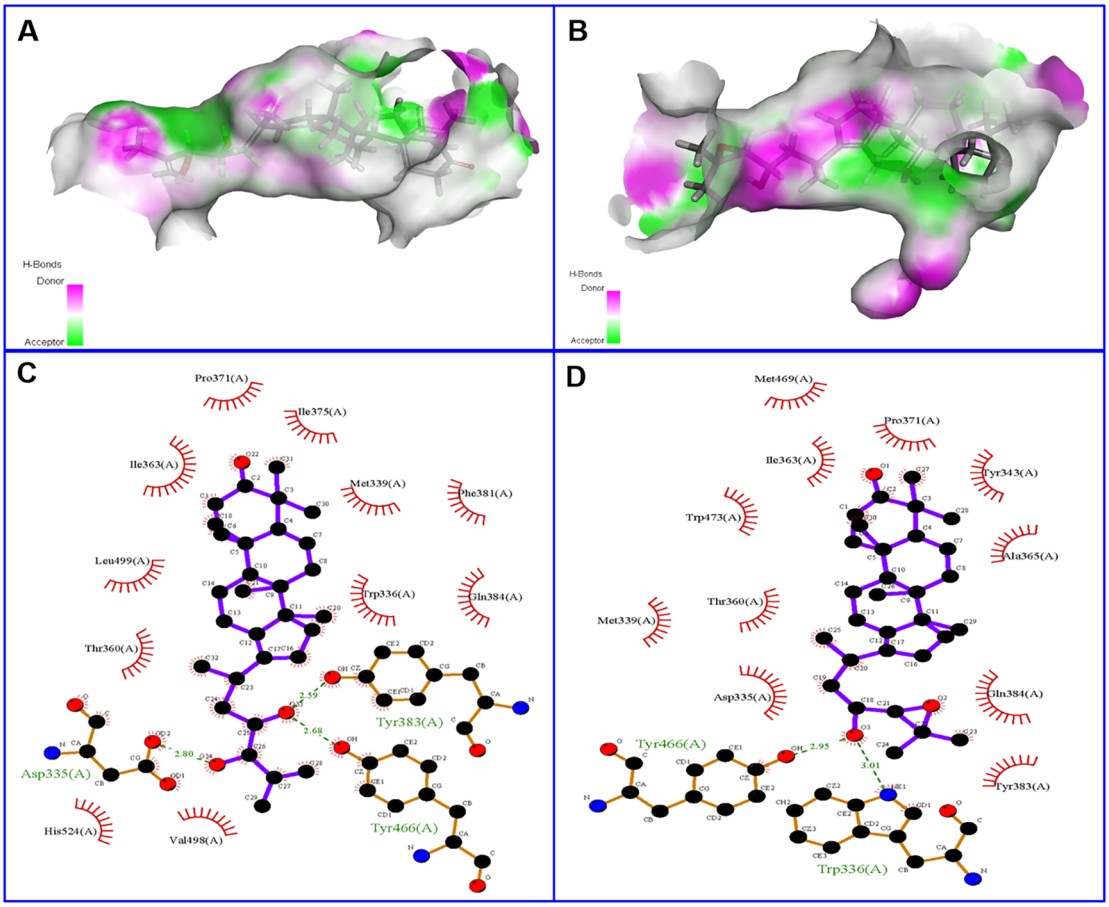

Fig. 4. (A-B) Compounds **4** (A) and **5** (B) could be bonded into the catalytic cavity of sEH. (C-D) 2D interactions of compounds **4** (C) and **5** (D) with sEH. The green dotted lines expressed hydrogen bonds.

Table 3
Interaction information of compounds **4** and **5** with sEH.

Compounds	Interaction amino acids	Hydrogen bonds	Lowest binding energy (kcal/mol)
4	Asp335, Trp336, Met339, Thr360, Ile363, Pro371, Ile375, Phe381, Tyr383, Gln384, Tyr466, Val498, Leu499, His524	Asp335, Tyr383, Tyr466	−36.45
5	Asp335, Trp336, Met339, Tyr343, Thr360, Ala365, Ile363, Pro371, Tyr383, Gln384, Met469, Tyr466, Trp473	Trp336, Tyr466	−40.52

were analyzed by molecular docking according to the previous method [23]. The 3D structure of compounds **4** and **5** were optimized at CHARMm force field by Discovery Studio software (BIOVIA Inc., San Diego, USA). The interactions of compounds **4** and **5** with sEH were analyzed at CHARMm force field using the CDOCKER protocol of Discovery Studio [35,36].

4.5. Molecular dynamics

Molecular dynamics (MD) simulation of compound **5** with sEH was calculated by GROMACS using the AMBER99SB force field [19,20,22]. The restrained electrostatic potential charges of ligand were calculated at B3LYP/6-31 + G (d, p) level by the Gaussian 09 program. Then, the starting topology of the ligand was generated by antechamber and ACPYPE programs. The complex of compound **5** with sEH was placed centrally in a rectangular box with a size of 1.2 nm. After the assembly, the steepest descent energy minimization was applied to relax the system. Then, NVT and NPT were used to equilibrate the system at the constant temperature of 300 K and the constant pressure of 1 bar, respectively. MD interaction of compound **5** and sEH was calculated at 300 K and 1 bar pressure for 10 ns after equilibration. The trajectory file was analyzed by GROMACS to obtain the root mean square deviation

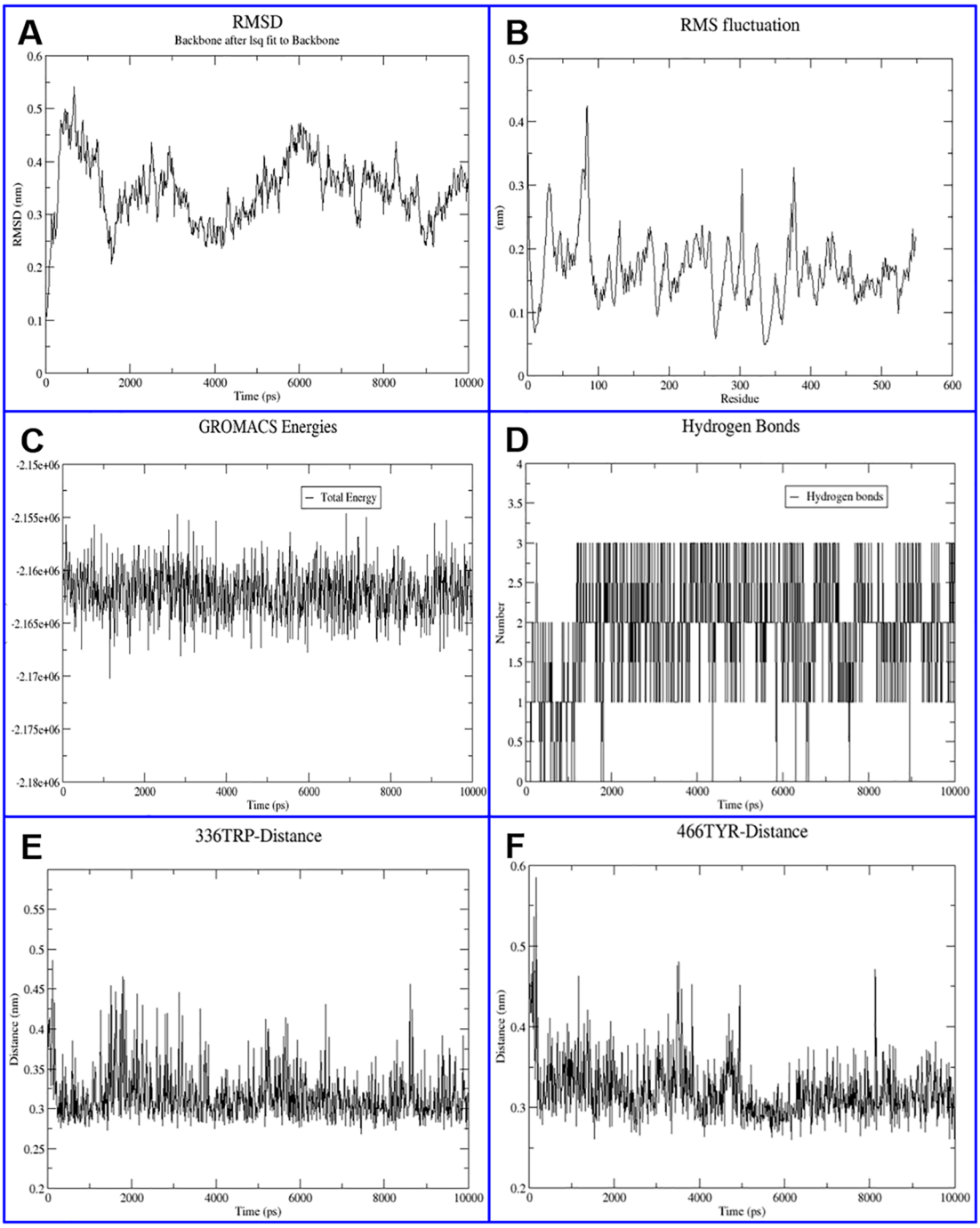

Fig. 5. The RMSD (A), RMSF (B), potential energy (C), and hydrogen bond number (D) of compound **5** with sEH. The distance of compound **5** with amino acid residues Trp336 (E) and Tyr466 (F).

(RMSD), root mean square fluctuations (RMSF). The total number of intermolecular hydrogen bonds (HB) formed between compound **5** and sEH and HB distribution for the system.

Declaration of Competing Interest

The authors declare that they have no known competing financial interests or personal relationships that could have appeared to influence the work reported in this paper.

Acknowledgments

This work was supported by National Natural Science Foundation of China (No. 81703769), Revolutionizing Innovative, Visionary Environmental Health Research Program of the National Institutes of Environmental Health Sciences (R35 ES030443-01), Superfund Basic Research Program of the National Institutes of Environmental Health Sciences (P42 ES04699), and Dalian Young Star of Science and Technology.

References

[1] J.K. Beetham, T. Tian, B.D. Hammock, cDNA cloning and expression of a soluble epoxide hydrolase from human liver, Arch. Biochem. Biophys. 305 (1) (1993) 197–201.

[2] D.F. Grant, D.H. Storms, B.D. Hammock, Molecular cloning and expression of murine liver soluble epoxide hydrolase, J. Biol. Chem. 268 (23) (1993) 17628–17633.

[3] M. Decker, M. Adamska, A. Cronin, F. Di Giallonardo, J. Burgener, A. Marowsky, J.R. Falck, C. Morisseau, B.D. Hammock, A. Gruzdev, D.C. Zeldin, M. Arand, EH3 (ABHD9): the first member of a new epoxide hydrolase family with high activity for fatty acid epoxides, J. Lipid Res. 53 (10) (2012) 2038–2045.

[4] J.W. Newman, C. Morisseau, T.R. Harris, B.D. Hammock, The soluble epoxide hydrolase encoded by EPXH2 is a bifunctional enzyme with novel lipid phosphate phosphatase activity, P. Natl. Acad. Sci. USA 100 (4) (2003) 1558–1563.

[5] B.D. Przybyla-Zawislak, P.K. Srivastava, J. Vazquez-Matias, H.W. Mohrenweiser, J.E. Maxwell, B.D. Hammock, J.A. Bradbury, A.E. Enayetallah, D.C. Zeldin, D.F. Grant, Polymorphisms in human soluble epoxide hydrolase, Heterocycles 64 (2) (2003) 482–490.

[6] K.M. Wagner, C.B. McReynolds, W.K. Schmidt, B.D. Hammock, Soluble epoxide hydrolase as a therapeutic target for pain, inflammatory and neurodegenerative diseases, Pharmacol. Ther. 180 (2017) 62–76.

[7] Q. Ren, M. Ma, J. Yang, R. Nonaka, A. Yamaguchi, K. Ishikawa, K. Kobayashi, S. Murayama, S.H. Hwang, S. Saiki, W. Akamatsu, N. Hattori, B.D. Hammock, K. Hashimoto, Soluble epoxide hydrolase plays a key role in the pathogenesis of Parkinson's disease, P. Natl. Acad. Sci. USA 115 (25) (2018) E5815–E5823.

[8] L.J. Zhong, J.T. Zhou, D.W. Wang, X.J. Zou, Y.X. Lou, D. Liu, B. Yang, Y. Zhu, X.X. Li, Proteomics and bioinformatics analysis of mouse hypothalamic neurogenesis with or without EPHX2 gene deletion, Int. J. Clin. Exp. Pathol. 8 (10) (2015) 12634–12645.

[9] W.H. Schunck, A. Konkel, R. Fischer, K.H. Weylandt, Therapeutic potential of omega-3 fatty acid-derived epoxyeicosanoids in cardiovascular and inflammatory diseases, Pharmacol. Ther. 183 (2018) 177–204.

[10] A.I. Ostermann, M. Reutzel, N. Hartung, N. Franke, L. Kutzner, K. Schoenfeld, K.H. Weylandt, G.P. Eckert, N.H. Schebb, A diet rich in omega-3 fatty acids enhances expression of soluble epoxide hydrolase in murine brain, Prostaglandins Other Lipid Mediat. 133 (2017) 79–87.

[11] B.Q. Deng, Y. Luo, X. Kang, C.B. Li, C. Morisseau, J. Yang, K.S.S. Lee, J. Huang, D.Y. Hu, M.Y. Wu, A. Peng, B.D. Hammock, J.Y. Liu, Epoxide metabolites of arachidonate and docosahexaenoate function conversely in acute kidney injury involved in GSK3 beta signaling, P. Natl. Acad. Sci. USA 114 (47) (2017) 12608–12613.

[12] Q. Ren, Soluble epoxide hydrolase inhibitor: a novel potential therapeutic or prophylactic drug for psychiatric disorders, Front. Pharmacol. 10 (2019) 420.

[13] W.C. Wang, J. Yang, J.A. Zhang, Y.X. Wang, S.H. Hwang, W.P. Qi, D.B. Wan, D. Kim, J. Sun, K.Z. Sanidad, H.X. Yang, Y. Park, J.Y. Liu, X.F. Zhao, X.H. Zheng, Z.H. Liu, B.D. Hammock, G.D. Zhang, Lipidomic profiling reveals soluble epoxide hydrolase as a therapeutic target of obesity-induced colonic inflammation, P. Natl. Acad. Sci. USA 115 (20) (2018) 5283–5288.

[14] D.Y. Xu, B.B. Davis, Z.H. Wang, S.P. Zhao, B. Wasti, Z.L. Liu, N. Li, C. Morisseau, N. Chiamvimonvat, B.D. Hammock, A potent soluble epoxide hydrolase inhibitor, t-AUCB, acts through PPAR gamma to modulate the function of endothelial progenitor cells from patients with acute myocardial infarction, Int. J. Cardiol. 167 (4) (2013) 1298–1304.

[15] A.B. Eldrup, F. Soleymanzadeh, N.A. Farrow, A. Kukulka, S. De Lombaert, Optimization of piperidyl-ureas as inhibitors of soluble epoxide hydrolase, Bioorg. Med. Chem. Lett. 20 (2) (2010) 571–575.

[16] N.M. Wolf, C. Morisseau, P.D. Jones, B. Hock, B.D. Hammock, Development of a high-throughput screen for soluble epoxide hydrolase inhibition, Anal. Biochem. 355 (1) (2006) 71–80.

[17] W.S. Xie, X.Y. Tang, Q. Lu, R.S. Ames, S.J. Ratcliffe, H. Li, Development of a high throughput cell-based assay for soluble epoxide hydrolase using BacMam technology, Mol. Biotechnol. 45 (3) (2010) 207–217.

[18] V. Burmistrov, C. Morisseau, T.R. Harris, G. Butov, B.D. Hammock, Effects of adamantane alterations on soluble epoxide hydrolase inhibition potency, physical properties and metabolic stability, Bioorg. Chem. 76 (2018) 510–527.

[19] J.H. Kim, I.S. Cho, J. Ryu, J.S. Lee, J.S. Kang, S.Y. Kang, Y.H. Kim, In vitro and in silico investigation of anthocyanin derivatives as soluble epoxide hydrolase inhibitors, Int. J. Biol. Macromol. 112 (2018) 961–967.

[20] J.H. Kim, Y.D. Jo, C.H. Jin, Isolation of soluble epoxide hydrolase inhibitor of capsaicin analogs from *Capsicum chinense* Jacq. cv. Habanero, Int. J. Biol. Macromol. 135 (2019) 1202–1207.

[21] A. Lukin, J. Kramer, M. Hartmann, L. Weizel, V. Hernandez-Olmos, K. Falahati, I. Burghardt, N. Kalinchenkova, D. Bagnyukova, N. Zhurilo, J. Rautio, M. Forsberg, J. Ihalainen, S. Auriola, J. Leppanen, I. Konstantinov, D. Pogoryelov, E. Proschak, D. Dar'in, M. Krasavin, Discovery of polar spirocyclic orally bioavailable urea inhibitors of soluble epoxide hydrolase, Bioorg. Chem. 80 (2018) 655–667.

[22] N.P. Thao, J.H. Kim, B.T.T. Luyen, N.T. Dat, Y.H. Kim, In silico investigation of cycloartane triterpene derivatives from *Cimicifuga dahurica* (Turcz.) Maxim. roots for the development of potent soluble epoxide hydrolase inhibitors, Int. J. Biol. Macromol. 98 (2017) 526–534.

[23] Z.B. Liu, C.P. Sun, J.X. Xu, C. Morisseau, B.D. Hammock, F. Qiu, Phytochemical constituents from *Scutellaria baicalensis* in soluble epoxide hydrolase inhibition: kinetics and interaction mechanism merged with simulations, Int. J. Biol. Macromol. 133 (2019) 1187–1193.

[24] I.H. Kim, F.R. Heirtzler, C. Morisseau, K. Nishi, H.J. Tsai, B.D. Hammock, Optimization of amide-based inhibitors of soluble epoxide hydrolase with improved water solubility, J. Med. Chem. 48 (10) (2005) 3621–3629.

[25] M. Manickam, T. Pillaiyar, P. Boggu, E. Venkateswararao, H.B. Jalani, N.D. Kim, S.K. Lee, J.S. Jeon, S.K. Kim, S.H. Jung, Discovery of enantioselectivity of urea inhibitors of soluble epoxide hydrolase, Eur. J. Med. Chem. 117 (2016) 113–124.

[26] N.R. McElroy, P.C. Jurs, C. Morisseau, B.D. Hammock, QSAR and classification of murine and human soluble epoxide hydrolase inhibition by urea-like compounds, J. Med. Chem. 46 (6) (2003) 1066–1080.

[27] K.S.S. Lee, J.Y. Liu, K.M. Wagner, S. Pakhomova, H. Dong, C. Morisseau, S.H. Fu, J. Yang, P. Wang, A. Ulu, C.A. Mate, L.V. Nguyen, S.H. Hwang, M.L. Edin, A.A. Mara, H. Wulff, M.E. Newcomer, D.C. Zeldin, B.D. Hammock, Optimized inhibitors of soluble epoxide hydrolase improve *in vitro* target residence time and *in vivo* efficacy, J. Med. Chem. 57 (16) (2014) 7016–7030.

[28] K. Hiesinger, J.S. Kramer, J. Achenbach, D. Moser, J. Weber, S.K. Wittmann, C. Morisseau, C. Angioni, G. Geisslinger, A.S. Kahnt, A. Kaiser, A. Proschak, D. Steinhilber, D. Pogoryelov, K. Wagner, B.D. Hammock, E. Proschak, Computer-aided selective optimization of side activities of talinolol, Acs Med. Chem. Lett. 10 (6) (2019) 899–903.

[29] L. Oster, S. Tapani, Y.F. Xue, H. Kack, Successful generation of structural information for fragment-based drug discovery, Drug Discov. Today 20 (9) (2015) 1104–1111.

[30] J. Pilger, A. Mazur, P. Monecke, H. Schreuder, B. Elshorst, S. Bartoschek, T. Langer, A. Schiffer, I. Krimm, M. Wegstroth, D. Lee, G. Hessler, K.U. Wendt, S. Becker, C. Griesinger, A combination of spin diffusion methods for the determination of protein-ligand complex structural ensembles, Angew. Chem. Int. Edit. 54 (22) (2015) 6511–6515.

[31] K. Takai, N. Chiyo, T. Nakajima, T. Nariai, C. Ishikawa, S. Nakatani, A. Ikeno, S. Yamamoto, T. Sone, Three-dimensional rational approach to the discovery of potent substituted cyclopropyl urea soluble epoxide hydrolase inhibitors, Bioorg. Med. Chem. Lett. 25 (8) (2015) 1705–1708.

[32] T.T. Liu, X.K. Huo, X.G. Tian, J.H. Liang, J. Yi, X.Y. Zhang, S. Zhang, L. Feng, J. Ning, B.J. Zhang, C.P. Sun, X.C. Ma, Demethylbellidifolin isolated from *Swertia bimaculate* against human carboxylesterase 2: Kinetics and interaction mechanism merged with docking simulations, Bioorg. Chem. 90 (2019) 103101.

[33] C. Wang, X.K. Huo, Z.L. Luan, F. Cao, X.G. Tian, X.Y. Zhao, C.P. Sun, L. Feng, J. Ning, B.J. Zhang, X.C. Ma, Alismanin A, a triterpenoid with a C_{34} skeleton from *Alisma orientale* as a natural agonist of human pregnane X receptor, Org. Lett. 19 (20) (2017) 5645–5648.

[34] J. Yi, R. Bai, Y. An, T.T. Liu, J.H. Liang, X.G. Tian, X.K. Huo, L. Feng, J. Ning, C.P. Sun, X.C. Ma, H.L. Zhang, A natural inhibitor from *Alisma orientale* against human carboxylesterase 2: kinetics, circular dichroism spectroscopic analysis, and docking simulation, Int. J. Biol. Macromol. 133 (2019) 184–189.

[35] Z.L. Luan, X.K. Huo, P.P. Dong, X.G. Tian, C.P. Sun, X. Lv, L. Feng, J. Ning, C. Wang, B.J. Zhang, X.C. Ma, Highly potent non-steroidal FXR agonists protostane-type triterpenoids: structure-activity relationship and mechanism, Eur. J. Med. Chem. 182 (2019) 111652.

[36] J.H. Liang, Z.L. Luan, X.G. Tian, W.Y. Zhao, Y.L. Wang, C.P. Sun, X.K. Huo, S. Deng, B.J. Zhang, Z.J. Zhang, X.C. Ma, Uncarialins A-I, monoterpenoid indole alkaloids from *Uncaria rhynchophylla* as natural agonists of the 5-HT_{1A} receptor, J. Nat. Prod. 82 (12) (2019) 3302–3310.